ACS APPLIED MATERIALS & INTERFACES

Research Article

www.acsami.org

Carbon/Ternary Alloy/Carbon Optical Stack on Mylar as an Optical Data Storage Medium to Potentially Replace Magnetic Tape

Hao Wang,[†] Barry M. Lunt,*[,‡] Richard J. Gates,[†] Matthew C. Asplund,[†] V. Shutthanandan,[§] Robert C. Davis,[∥] and Matthew R. Linford*[,†]

[†]Department of Chemistry and Biochemistry, [‡]Department of Information Technology, and [∥]Deparment of Physics and Astronomy, Brigham Young University, Provo, Utah 84602, United States

[§]Environmental Molecular Sciences Laboratory, Pacific Northwest National Laboratory, Richland, Washington 99352, United States

ABSTRACT: A novel write-once-read-many (WORM) optical stack on Mylar tape is proposed as a replacement for magnetic tape for archival data storage. This optical tape contains a cosputtered bismuth−tellurium−selenium (BTS) alloy as the write layer sandwiched between thin, protective films of reactively sputtered carbon. The composition and thickness of the BTS layer were confirmed by Rutherford Backscattering (RBS) and atomic force microscopy (AFM), respectively. The C/BTS/C stack on Mylar was written to/marked by 532 nm laser pulses. Under the same conditions, control Mylar films without the optical stack were unaffected. Marks, which showed craters/movement of the write material, were characterized by optical microscopy and AFM. The threshold laser powers for making marks on C/BTS/C stacks with different thicknesses were explored. Higher quality marks were made with a 60× objective compared to a 40× objective in our marking apparatus. The laser writing process was simulated with COMSOL.

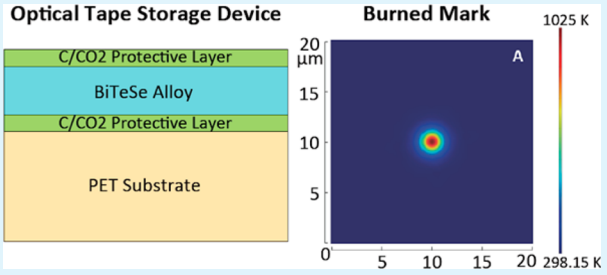

KEYWORDS: *data storage, optical tape, bismuth, tellurium, selenium, carbon, sputter*

INTRODUCTION

Magnetic tape has a long history as an information storage medium because of its high writing/reading efficiency, low cost, and reliability.[1] Accordingly, it remains one of the most popular tools for backing up data in libraries, corporations, government agencies, and scientific research institutions.[2] However, despite its broad appeal, magnetic tape has a rather short lifetime. Indeed, most organizations typically begin to rotate it after only seven years of use—the tape undergoes a plastic deformation (a stretching) each time it is read,[3,4] and with time delamination of the write layer from the underlying substrate can occur. Magnetic tape is also subject to degradation of the signal amplitude as a function of the relaxation of the magnetic domains, which process is accelerated by temperature. Additionally, it is susceptible to various interferences, raising the risk of damage or loss of stored information. Because of these disadvantages, an optically based tape, which might employ a thin metal film as a data storage medium and might be written and read with a laser might be a promising substitute.[5] As optical, instead of magnetic, properties would dominate the information storage mechanism in this scenario, data could be stored at approximately the same density, but for a much longer period of time, and in a manner that might be less susceptible to diverse interferences.

Low melting point metals in thin film form, including tellurium, bismuth, and lead, are promising for optical data storage devices. Carlson et al. first investigated the possibility of making high-resolution recordings on thin films of lead using a He−Ne laser.[6] Terao et al. successfully marked thin films of bismuth, tellurium, selenium, and tin using an argon ion laser.[7] Li and co-workers demonstrated that the product of tellurium degradation under severe environmental conditions, TeO_x, is an alternative recording medium for optical storage devices.[8] Some of us recently reported a DVD that consists of a Te write layer sandwiched between two reactively sputtered carbon films.[9] This latter work was funded by Millenniata (American Fork, UT, www.mdisc.com), which sells a DVD that, based on established longevity tests, should last more than 1000 years. Millenniata also recently released a Blu-ray disc that is similarly expected to have exceptional longevity.

Low melting point metal alloys have also been investigated as a means of improving the properties of single element thin films. Terao found that the oxidation resistance of tellurium thin films was enhanced by introducing selenium into them.[10] In a later study, he demonstrated that the addition of some specific metals such as bismuth or lead to a Te−Se alloy can improve the film's resistance to cracking.[11] Clearly the much higher toxicity of Pb compared to Bi makes it less preferred in this application. Lou et al. also successfully prepared tellurium alloy disks that showed satisfactory environmental stability.[12]

Given the widespread use of magnetic tape and the potential of low melting point metal alloys as recording media, we sought

Received: May 6, 2013
Accepted: August 5, 2013
Published: August 21, 2013

   dx.doi.org/10.1021/am401693u | *ACS Appl. Mater. Interfaces* 2013, 5, 8407−8413

to fabricate and characterize a novel write-once-read-many (WORM) optical tape using a carbon/bismuth−tellurium−selenium/carbon (C/BTS/C) sandwich as the recording layer. The sandwich structure was prepared on a Mylar (biaxially oriented polyethylene terephthalate (PET)) substrate by reactive sputtering of carbon in carbon dioxide and by cosputtering the BTS film from bismuth and tellurium/selenium targets (see Figure 1). This stack is more complex

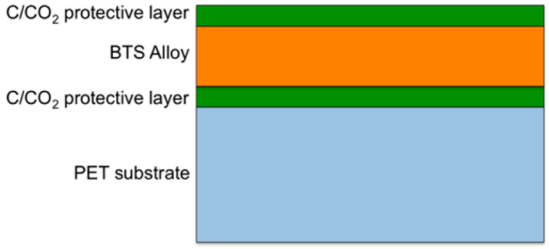

Figure 1. Schematic of the C/BTS/C optical stack on Mylar (PET substrate).

than the one we previously reported as the write layer for a WORM-type DVD.[9] The two carbon layers were employed as protective thin films and were reactively sputtered because of the high degree of residual stress that is typically present in undoped, sputtered carbon films.[13,14] Because sputtered films often show excellent adhesion to substrates we anticipated that this sandwich structure would adhere very well to Mylar, which has been confirmed.[15]

Herein, we report the deposition, characterization, and marking of a C/BTS/C optical stack on Mylar as a potential replacement for magnetic tape. Atomic force microscopy (AFM) provided BTS and carbon film thicknesses and Rutherford Backscattering (RBS) gave amounts of Bi, Te, Se, O, and film void fractions. AFM and optical microscopy were used to characterize the morphologies of the marks. The threshold for marking the material at a series of laser powers is given, and the write process is modeled using COMSOL. This work is a proof-of-concept study that is a continuation of our efforts to develop and understand materials for permanent data storage, and is related to other work we have undertaken on laser marking of surfaces.[16−20]

EXPERIMENTAL SECTION

Sputter Deposition. Sputtered/cosputtered C/BTS/C optical stacks were deposited simultaneously onto 20 μm Mylar films for laser marking and native oxide-terminated single crystal Si (100) substrates for AFM and RBS characterization. All substrates were cleaned with acetone, deionized water, isopropanol, and by plasma (1 min air plasma in a Harrick PDC-32G plasma cleaner, Harrick Plasma, Ithaca, NY) before deposition. Magnetron sputtering/cosputtering of the BTS and C/CO_2 layers took place in a three-target PVD 75 sputter deposition system (Kurt J. Lesker, Clariton, PA). Carbon was reactively, DC sputtered from a 99.999% carbon target (Plasmaterials, Inc., Livermore, CA) in an atmosphere of 10% CO_2 in argon at 400 W for 20 min, where the ratio of CO_2 to Ar was controlled by mass flow controllers. The BTS thin film was deposited by DC cosputtering a 99.999% bismuth target at 10 W and a custom ordered Te−Se target (Te: 78.4 at.%, Se: 21.6 at.%, individual purities of Te and Se were 99.999%, Plasmaterials, Inc., Livermore, CA) at 20 W under Ar. The gas pressure for both depositions was 10^{-5} Torr prior to deposition and 10^{-3} Torr during deposition. Substrates were attached to a rotating platen (20 r/min) by double-sided Scotch tape. The platen was located about 30 cm above the sputtering guns. The thickness of the C/CO_2 film was 11 nm in all depositions, and the thicknesses of the BTS films ranged between 19.5 and 131 nm. The deposition rate was 0.55 nm/min for the C/CO_2 layer and 3.50 nm/min for the BTS layer.

Laser Writing Apparatus. Figure 2 represents our home-built laser writing apparatus. A diode pumped solid state (DPSS) Nd:YAG

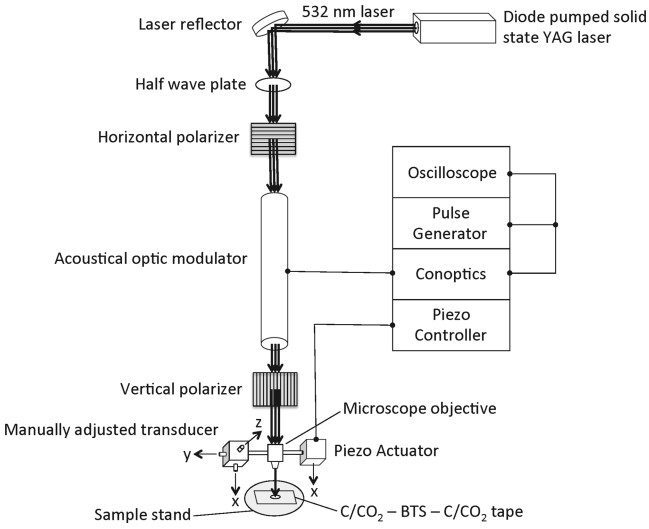

Figure 2. Schematic of the laser writing apparatus.

laser together with a MPC6000 DPSS laser power supply (both purchased from Laser Quantum Ltd., Stockport, England) were used as the 532 nm laser source. The laser beam was reflected by a KM100 reflector (Thorlabs Inc., NJ) to a 532 nm half-wave plate (Thorlabs, Newton, NJ), through which the laser beam polarization angle could be adjusted. A horizontal line polarizing cube beam splitter (Newport Corporation, CA), a 380 E.O. acoustical optic modulator (Conoptics Inc., Danbury, CT), and a vertical line polarizing cube beam splitter formed a "switch" to produce laser pulses. Both polarizing cube beam splitters filter out 95% of the incident laser beam and let only the horizontal/vertical component of the remaining 5% of the laser beam through. When the modulator is given a certain voltage (turn-on mode) by a 214B pulse generator (Agilent Technologies, Englewood, CO), the modulator can convert horizontally polarized laser beams into vertically polarized ones so that they can pass through the vertical line polarizing cube; when the voltage is set back to zero (turn-off mode), the modulator does nothing to the laser beam so it is unable to pass through the vertical line polarizing cube. The two polarizing beam splitters not only polarize the laser beams but also buffer the sample from spikes in laser power. By turning on and off the modulator voltage, a laser pulse is generated. The laser pulse width was set to 100 ns on the pulse generator. The obtained laser pulse was then focused by a 40× or 60× microscope objective (Thorlabs) onto the sample surface. The position of the objective and its distance from the sample surface could be roughly tuned by a manually adjusted transducer and were finely tuned by a piezo actuator (Physik Instrumente L.P., Irvine, CA). A clean polycarbonate disc (600 um) was used as a sample stand, onto which samples were adhered with Scotch tape. The laser power could be tuned by either rotating the half-wave plate to control the laser beam passing through the first polarizing beam splitter or by adjusting the DPSS laser power supply. All laser powers were directly measured by a Newport 2935-C power meter.

Film Thickness Determination and Film Characterization. Film thicknesses (step height measurements) and laser mark cross sections were determined/confirmed using a Veeco Dimension V AFM (Digital Instruments Inc., Santa Barbara, CA) with the device in tapping mode. The AFM tips were n^+-silicon chips with 10 μm needles purchased from Nanosensors (Neuchatel, Switzerland). A shard of silicon with about 1.5 nm native oxide was coated simultaneously with one or more Mylar substrates in the PVD 75. Prior to deposition, a line was drawn on the Si surface with a felt tip (Sharpie) pen. After

coating, the line was rinsed off with isopropanol, which resulted in a clean step edge for AFM height measurements. The AFM step height measurements were calibrated against a 100 nm SiO_2 standard. Thicknesses of all samples reported in this work were confirmed by AFM height measurements. Laser mark sizes were measured by optical microscopy (BX60, Olympus America Inc., Center Valley, PA). The composition of the BTS layer was determined by RBS as described previously.[21] The Void Fraction in the BTS film was modeled as hydrogen because RBS is sensitive to heavier elements, but not hydrogen, which is too light to reflect helium ions to the detector. This approach is commonly used in RBS to model voids in films.

Laser Writing Simulation. The laser writing process on a BTS film was modeled using COMSOL Multiphysics (Version 4.0 a, COMSOL, Inc., Burlington, MA). The laser pulse was simulated as a circular, Gaussian pulse with a duration of 100 ns, power of 10 mW, and diameter of 478 nm impinging on a 40 nm thick, 20 × 20 μm BTS film. No other film was present, that is, the mylar/C/BTS/C film was modeled here as a single, freestanding BTS layer. Simulations were performed for the 40× and 60× objectives using their corresponding NA (numerical aperture) values.

Equation 1, $f(x, y)$, describes the Gaussian form of the laser spot

$$f(x, y) = \frac{Q_0(1 - R_c)A_c}{2\pi \cdot \sigma_x \cdot \sigma_y} e^{-\left(\frac{(x-x_0)^2}{2\sigma_x^2} + \frac{(y-y_0)^2}{2\sigma_y^0}\right)} \quad (1)$$

where Q_0 is the laser power, A_c is the light absorption coefficient of the BTS alloy, R_c is the light reflection coefficient of the BTS alloy, σ_x and σ_y are the x- and y-diameters of the laser spot, and x_0 and y_0 are the x- and y-coordinates of the center of the laser spot, which are both 10 μm here. The BTS film absorption coefficient (A_c) and refraction coefficient (R_c) were measured with an M-2000 spectroscopic ellipsometer (J. A. Woollam Co., Inc., Lincoln, NE). The exponential decay of the laser power as a function of the thickness of the BTS film, z, as the pulse travels into the BTS alloy was represented by eq 2

$$d(z) = e^{-A_c z} \quad (2)$$

Equation 3 ($w(t)$) describes the square-wave function that provides a series of 100 ns wide laser pulses with a 100 ns break between them

$$w(t) = \mathrm{abs}\left(\cos \frac{\mathrm{floor}\left(\frac{t}{T}\right)}{2}\pi\right) \quad (3)$$

where t is a certain time during the simulation process, T is the 100 ns pulse width, abs(x) is a function that takes the absolute value of its argument, and floor(x) is a function that rounds its argument to the next integer in the direction of negative infinity. The laser writing process could then be simulated by multiplying these functions together

$$p(x, y, z, t) = f(x, y)\, d(z)\, w(t) \quad (4)$$

The time scale for the simulation is 200 ns, which is made up of the 100 nm laser pulse and the response of the material thereafter. The simulation does not include phase changes, meaning that the BTS material will remain as a solid throughout the entire process even if the temperature exceeds the BTS melting point.

RESULTS AND DISCUSSION

1. Characterization of the Recording Layer. BTS films were deposited onto model silicon substrates for characterization by AFM and RBS. Figure 3A shows a typical AFM step height profile of a BTS film. The reasonably flat regions on both sides of the step allowed its thickness to be determined. Figure 3B shows RBS of a BTS thin film. This latter analysis reveals a Si edge that becomes a step toward lower channel number (energy) and represents the silicon substrate, with three peaks well separated from the substrate signal that increase in energy with increasing atomic mass. This film is

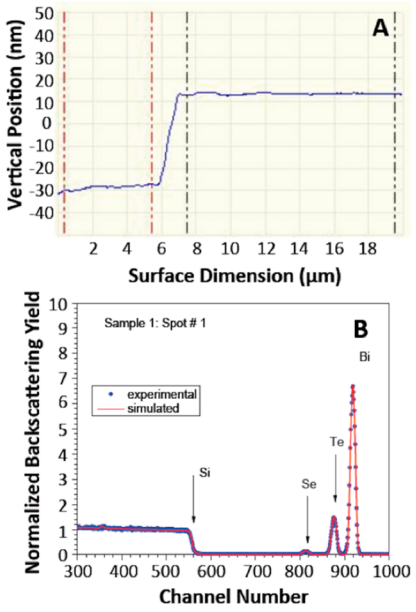

Figure 3. Analysis of a BTS film by (A) AFM step height measurement (for a 42.0 nm film), and (B) RBS. In panel A, the average position between the red vertical lines was subtracted from the average position between the black vertical lines to obtain the film thickness.

nearly ideal for RBS analysis as it is composed of heavier elements on a lighter substrate. Based on modeling of the RBS spectra of four separately deposited films, the composition of the BTS layers was determined to be 39.0 ± 1.7 at.% Bi, 22.7 ± 1.0 at.% Te, 5.8 ± 0.3 at.% Se, 11.5 ± 1.8 at.% O, and 20.9 ± 2.8 at.% void (errors here are standard deviations).

2. COMSOL Simulation of Laser Writing on a BTS Film. We simulated the time-dependent temperature distribution and estimated the corresponding mark dimensions for our laser marking process in the BTS film. Figure 4A shows the temperature profile across the film surface at 100 ns, which is the length of the laser pulse, that is, at the end of the laser pulse. As expected, the maximum temperature in the film is predicted to be at the center of the laser pulse. Figure 4B shows a series of time dependent temperature profiles along the central line, which goes across the top of the BTS film. These indicate that the temperature reaches a maximum at about 100 ns.

Bi, Te, and Se have low melting points (m.p.) of 544.6 K, 722.7 K, and 493.7 K, respectively.[22] Based on the atom percentages of these elements in the recording layer determined by RBS (vide supra), a rough (weighted average) estimate of the melting point of the BTS layer is 600 K. According to the temperature distribution at 100 ns (see Figure 4B), a region approximately 2 μm in diameter exceeds the material's melting point. That is, we can expect that the mark diameter will be on the order of 2 μm.

3. Effects of Laser Power on the Mark Size, Substrate, and Threshold Power. Figure 5A–E shows optical micrographs of typical marks made by laser pulses with powers ranging from 6 to 19 mW on a 142 nm (11 + 120 + 11 nm) C/BTS/C sandwich. We focus here on lower laser powers (under 20 mW) because they yield smaller spots that would be more advantageous for data storage. Each mark is the result of a single laser shot. All of the marks are moderately deformed circular/elliptical holes that result from absorbance of laser power by the recording layer, which is followed by melting and

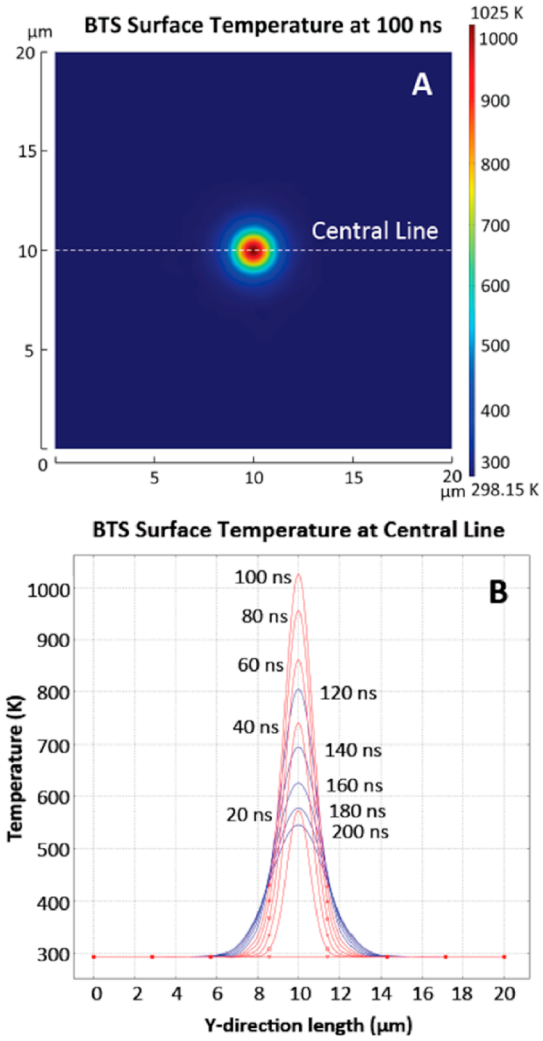

Figure 4. COMSOL simulation of the (A) temperature distribution of the BTS surface, and (B) temperature profile at the central line of the BTS surface after one 100 ns laser shot for the 40× objective.

migration of the BTS alloy. We attribute the somewhat elliptical nature of the marks to imprecisions in the home-built apparatus used to make them (see Figure 2). The heat affected zone (HAZ), a bright annular region around the hole, is considered to be the collaborative product of thermal conduction away from the focused laser spot and accumulation of melted BTS material away from the pits. In control experiments, no marks are observed on bare Mylar substrates at these laser powers unless the C/BTS/C layer is present.

HAZ, a critical factor that defines data density in magnetic and optical data storage, determines how close one mark can be placed to another. Smaller HAZs can help reduce intersymbol interference (ISI) between marks and thus increase data density, which is one of the main goals for developing today's data storage devices. Therefore, small HAZ is preferred in this optical tape. To understand the relationship between laser power and HAZ, the inner diameter (ID) and outer diameter (OD) of the HAZs from marks made with laser powers ranging from 6−19 mW were measured by optical microscopy (see Figures 5 and 6). As expected, both the IDs and ODs of the

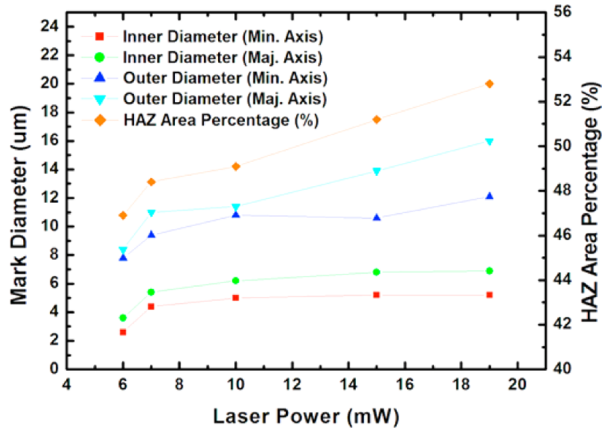

Figure 6. Mark dimensions (major axes and minor axes of the ellipses) and the percentage of the HAZ as a function of the entire area of the mark.

HAZs increase as laser power increased. Also as shown in Figure 6, the area of the HAZ remains at about 50% of the total area of the marks although it is a little less for the marks made with the lower laser powers.

When a laser beam just barely burns through the C/BTS/C recording layer without substantially penetrating the Mylar substrate, the resulting mark is defined as a threshold mark and the corresponding laser power is termed the threshold power. In Figure 5A, the central area of the 6 mW mark is white and shiny, indicating that the Mylar substrate is reflecting light back to the camera. On the other hand, in Figure 5B−5E, the central areas of the marks are dark, meaning that the Mylar has been substantially damaged and no longer reflects light. Obviously at lower laser powers, less substrate damage is expected. According to this definition, 6 mW is near the threshold power of a 142 nm sample, and the crater we observe approximates a threshold mark.

The thickness of the C/BTS/C recording layer should significantly affect the threshold power needed to write to it.

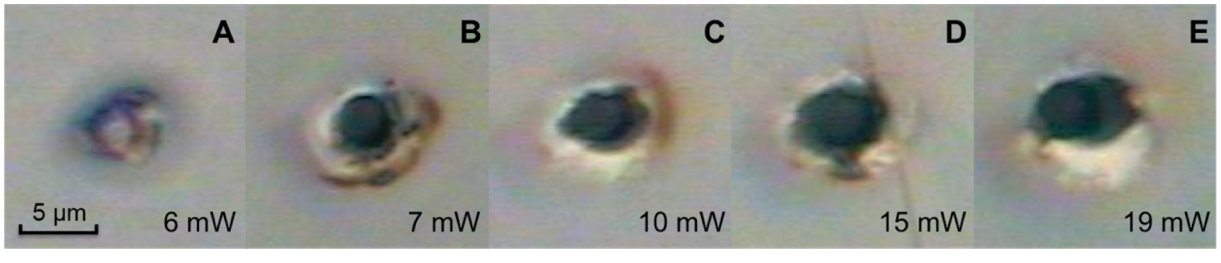

Figure 5. Series of marks made with single pulses of a 532 nm laser with different powers on a C/BTS/C film with dimensions of 11 nm, 120 nm, and 11 nm, respectively.

Accordingly, the threshold powers for recording layers with different thicknesses are plotted in Figure 7. Interestingly,

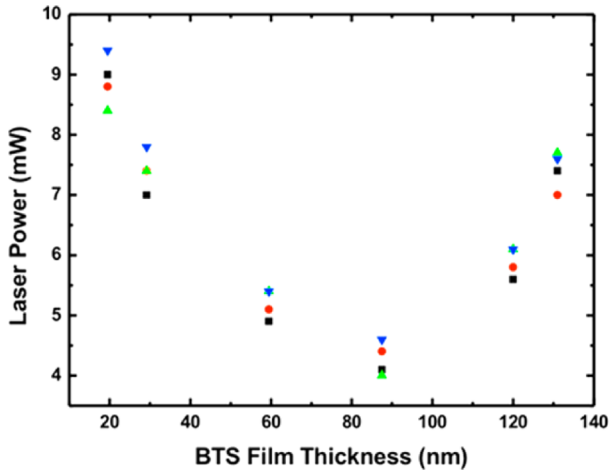

Figure 7. Threshold powers of C/BTS/C stacks on Mylar with different BTS alloy thicknesses. Each symbol type represents data taken from a different Mylar/C/BTS/C film.

instead of becoming steadily lower as the stack thickness decreases, the threshold power first decreases to about 4 mW, when the stack thickness is 87.5 nm, and then rises again as the stack thickness continues to decrease.

One might have expected that as the BTS layer decreased in thickness, the laser power required for melting it would also decrease, that is, that less power would be required to melt a thinner film. However, this effect must be balanced against the decreasing optical absorbance of the thinner film, which would suggest that a higher laser power would be required to melt it. The combination of these two effects appears to give the results in Figure 7, that is, that writing to either very thick or very thin films requires higher powers, but that lower laser powers can write to films with intermediate thicknesses.

As discussed before, the melting point of the BTS alloy (600 K) exceeds that of Mylar (about 518−523 K) and suggests that when the BTS film melts and moves it may affect the underlying Mylar substrate. Figure 8 shows top and cross-sectional views obtained by tapping mode AFM of a 6 mW (threshold) laser mark. The protuberance at the edge of the crater corresponds to the HAZ. By subtracting the recording layer thickness (142 nm) from the depth of the crater (174 nm) we determine that about 32 nm of the depth of the crater is a result of melting/movement/damage to the Mylar substrate. As expected, damage at this level is insufficient to significantly change the optical reflectivity of the Mylar substrate.

4. Influence of Objectives on Marks. The simulation above (see Figure 4), which was performed for the 40× objective, was repeated for a 60× objective. Very similar results were obtained in the two simulations.

But experimentally, the 60× objective gave very different results from the 40×. Figure 9 shows a series of marks made by laser pulses focused with a 60× objective on 142 nm (11 + 120 + 11 nm) C/BTS/C optical stacks. As expected, these 60× objective marks are more circular and have clearer edges than the previously made 40× objective marks. Mark diameters and HAZ area fractions are listed in Table 1. This time mark IDs fall below 3 μm, which is clearly desirable because smaller marks lead directly to higher mark density and larger information capacity. Indeed, at the lowest laser powers considered, the marks prepared with the 40× objective and measured to the outside of the HAZ are about 8 μm (Figure 6). Table 1 shows that the marks, including HAZ, made with the 60× objective are about 4 μm. Thus, for our home-built apparatus the possible information density along a linear track should approximately double for the 60× objective. On an areal basis, the information density would quadruple. These smaller mark sizes also show improved agreement with the COMSOL simulation (vide supra). Unlike the 40× objective marks, the dimensions of the 60× objective marks are both more consistent between different laser powers and much less correlated with laser power. In addition, the ODs of the 60× objective marks do not differ too much from their corresponding IDs. The negative effect of HAZs on marks is thus reduced by use of a higher magnification objective.

The laser power required for making 60× objective marks also drops sharply in comparison with the powers required to make 40× objective marks. According to Figure 9 and Table 1, laser pulses with powers as low as 1 mW can burn high quality marks. Unfortunately, because of the minimum power output of our laser and those of our home-built marking apparatus, we could not reduce the power further to explore laser pulses with energies below 1 mW. That is, we could never make threshold marks with the 60× objective as we did for the 40× spots (see Figure 7).

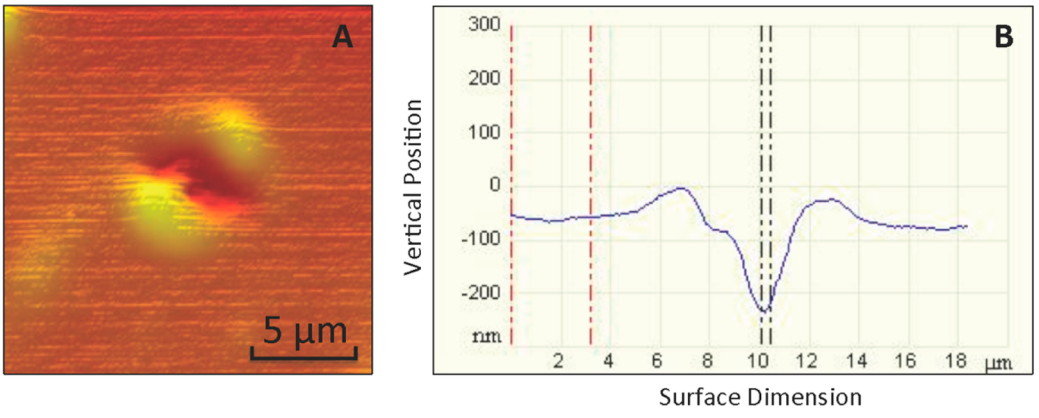

Figure 8. (A) AFM image of a 6 mW mark (B) AFM cross sectional image of this 6 mW mark showing mark depth of 174 nm. The mark depth is given by the difference between the average data value within the two red lines and the average value between the black lines.

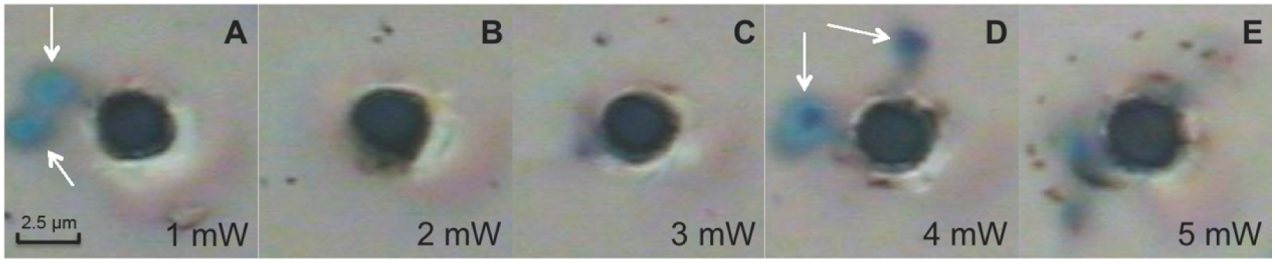

Figure 9. Optical micrographs of 60× objective marks at different powers of a 532 nm laser on a C/BTS/C film with dimensions of 11 nm, 120 nm, and 11 nm, respectively. The dark marks (primarily in A and D, note arrows) are presumably due to undesired reflections of the laser from other optical surfaces/components in the laser writing apparatus (see Figure 1). Improvements in that device should lead to a reduction in these unwanted marks.

Table 1. Diameters of 60× Objective Marks (Major Axes and Minor Axes) and the Percentage of the HAZs as a Function of the Entire Area of the Mark

	ID (μm)		OD (μm)		
laser power (mW)	maj. axis	min. axis	maj. axis	min. axis	HAZ area percentage (%)
1	2.9	2.7	4.5	4.3	43.8
2	2.9	2.4	4.2	3.4	41.7
4	2.9	2.9	4.1	4.0	46.6
6	3.2	2.4	4.3	4.0	44.5
8	2.5	2.2	3.9	3.6	43.9

5. Potential Data Density of an Optical Tape Storage Device. A straightforward calculation suggests that an optical tape storage medium should have roughly the same capacity as conventional magnetic linear tape-open (LTO) technology. Assuming (i) the same number of tracks as on LTO-6 (896), (ii) a linear density equal to that in the BD-MDisc from Millenniata (150 nm marks), and (iii) 820 m of tape (same as LTO-6), one obtains: 896 × 820 m × 1/150 nm/mark = 4.898 × 10^{12} marks (bits) = 612 GB (native). The stated capacity for the LTO-6, Generation 3, is 800 GB (native), so we are well within this same range of capacity.

6. Issues of Jitter and SNR. Because of the lack of any commercially available writer/reader for optical tape, we do not have any equipment capable of measuring the jitter values and signal-to-noise ratios (SNR) of our sample under current conditions. However, because of the similarity of our optical stack to that in a commercial optical data storage device that shows excellent performance and durability, good performance of this optical tape is also expected.[9] As jitter and SNR value are significant feature of a data storage device, we will be working to define these in the future.

7. Comments on the Imprecision of the Simulation and Marking Apparatus. In Section 2 (vide supra) we predicted the melting point of the BTS layer based on the melting points of its pure metallic components. This estimate was ultimately used to predict the size of the spots made in the COMSOL simulation. In reality, however, the melting point of the BTS write layer should be higher than the value predicted by the melting points of the pure metals because of the oxygen found by RBS in the film (see Section 1 above). That is, even though the RBS does not define the chemical state of the oxygen in the films, the presence of oxygen and the higher melting points of the oxides compared to the metals themselves (Bi_2O_3, TeO_2, and SeO_2 have melting points of 1090 K, 1006 K, and 613 K, respectively) suggest that the melting point of the film is higher than we predicted and that smaller marks could be made in this film. In addition, we note that the simulation was performed on a simplified version of the mylar/C/BTS/C optical stack—it was done on a freestanding BTS film. Clearly, in a real device, the substrate would act as a heat sink that would lower the maximum temperature obtainable during writing and therefore further reduce the size of the spot. Finally, we note that in spite of the relative sophistication of the apparatus we built to laser mark our surfaces (see Figure 2), it will not compare in capabilities or performance to a finely engineered read/write device, such as those sold commercially to read and write CD, DVD, and Blu-ray discs. For all of these reasons we are satisfied with the order-of-magnitude agreement we find between our experimental and simulated data.

CONCLUSIONS

We have made a novel write-once-read-many optical tape with a bismuth−tellurium−selenium write layer sandwiched between carbon films. AFM and RBS reveal and confirm desired film properties. A COMSOL simulation of the laser marking agreed reasonably well with experimental results. For the larger 40× objective, laser marks increase in size with laser power, and the threshold laser power for marking the BTS optical stack shows a minimum at around 85 nm. AFM of a laser mark is shown, which reveals a raised edge around the mark. Marks are smaller, more consistent in size, improved in shape, and less affected by laser power when made with a 60× objective. This is a proof-of-concept study. Because of (i) the positive results obtained herein and (ii) the fact that there are optical discs on the market with similar write layers performing at a high level, we believe that additional research is warranted in this area and that it could ultimately lead to a commercial optical tape solution for data storage.

AUTHOR INFORMATION

Corresponding Author

*E-mail: luntb@byu.edu (B.M.L.), mrlinford@chem.byu.edu (M.R.L.).

Notes

The authors declare no competing financial interest.

ACKNOWLEDGMENTS

We acknowledge the Departments of Chemistry and Biochemistry, Information Technology, and Physics and Astronomy at Brigham Young University for their support of this research. Part of this research was performed at EMSL, a national scientific user facility sponsored by the Department of Energy's Office of Biological and Environmental Research and located at Pacific Northwest National Laboratory.

REFERENCES

(1) Charap, S. H.; Lu, P.; He, Y. *IEEE Trans. Magn.* **1997**, *33* (1), 978−983.
(2) Engel, F.; Hammar, P.; Hess, R. A selected history of magnetic recording [online]; http://www.richardhess.com/tape/history/Engel_Hammar--Magnetic_Tape_History.pdf (accessed February 14, 2013).
(3) Carr, T.; Wachenschwanz, D. *IEEE Trans. Magn.* **1988**, *24* (6), 2961−2963.
(4) Ohta, T. *J. Optoelectron. Adv. Mater.* **2001**, *3* (3), 609−626.
(5) Larsen, T. L.; Woodard, F. E. *Annu. Tech. Conf. Proc. - Soc. Vac. Coaters* **1994**, *37*, 198−202.
(6) Carlson, C. O.; Stone, E.; Bernstein, H. L.; Tomita, W. K.; Myers, W. C. *Science* **1966**, *154*, 1550−1551.
(7) Terao, M.; Shigematsu, K.; Ojima, M.; Taniguchi, Y.; Horigome, S. *J. Appl. Phys.* **1979**, *50*, 6881−6886.
(8) Li, Q.; Gan, F. *Appl. Surf. Sci.* **2001**, *181*, 239−247.
(9) Abbott, J.; Niederhauser, T. L.; Hansen, D. P.; Perkins, R. T.; Bell, D. A.; Bard, E. C.; Lunt, B. M.; Worthington, M. O.; Miller, C. M.; Hyatt, D. F.; Asplund, M. C.; Jiang, G.; Linford, M. R.; Vanfleet, R. R.; Davis, R. C. *ACS Appl. Mater. Interfaces* **2010**, *2*, 2373−2376.
(10) Terao, M.; Horigome, S.; Shigematsu, K.; Miyauchi, Y.; Nakazawa, M. *Proc. Soc. Photo-Opt. Instrum. Eng.* **1983**, *382*, 276−281.
(11) Terao, M.; Horigome, S.; Shigematsu, K.; Miyauchi, Y.; Nakazawa, M. *J. Appl. Phys.* **1987**, *62*, 1029−1034.
(12) Lou, D.; Blom, G.; Kenney, G. *J. Vac. Sci. Technol.* **1981**, *18*, 78−86.
(13) Taylor, C. A.; Wayne, M. F.; Chiu, W. K. S. *Thin Solid Films* **2003**, *429*, 190−200.
(14) Ager, J. W., III. *Mater. Res. Soc. Symp. Proc.* **1995**, *383*, 143−151.
(15) Lunt, B. M.; Pearson, A.; Davis, R.; Wang, H.; Jamieson, S.; Linford, M. R. *Proc. Int. Symp. Opt. Memory* **2012**, 84−85.
(16) Jiang, G.; Rivera, F.; Kanyal, S. S.; Davis, R. C.; Vanfleet, R.; Lunt, B. M.; Shutthanandan, V.; Linford, M. R. *Opt. Eng.* **2011**, *50* (1), 015201/1−015201/10.
(17) Lunt, B. M.; Buntel, C. J.; Linford, M. R. *J. Adv. Mater.* **2009**, *41* (4), 22−27.
(18) Saini, G.; Gates, R.; Asplund, M. C.; Blair, S.; Attavar, S.; Linford, M. R. *Lab Chip* **2009**, *9*, 1789−1796.
(19) Yang, L.; Shirahata, N.; Saini, G.; Zhang, F.; Pei, L.; Asplund, M. C.; Kurth, D.; Ariga, K.; Sautter, K.; Nakanishi, T.; Smentkowski, V.; Linford, M. R. *Langmuir* **2009**, *25* (10), 5674−5683.
(20) Zhang, F.; Gates, R. J.; Smentkowski, V. S.; Natarajan, S.; Gale, B. K.; Watt, R. K.; Asplund, M. C.; Linford, M. R. *J. Am. Chem. Soc.* **2007**, *129* (30), 9252−9253.
(21) Jensen, D. S.; Kanyal, S. S.; Madaan, N.; Hancock, J. M.; Dadson, A. E.; Vail, M. A.; Vanfleet, R.; Shutthanandan, V.; Zhu, Z.; Engelhard, M. H.; Linford, M. R. *Surf. Interface Anal.* **2013**, *45* (8), 1273−1282.
(22) *Periodic Table of Elements*; Los Alamos National Laboratory: Los Alamos, NM; http://periodic.lanl.gov (accessed February 14, 2013).